Enhanced Fault-Tolerant Model Predictive Current Control for a Five-Phase PM Motor With Continued Modulation

Tao Tao, Wenxiang Zhao, *Senior Member, IEEE*, Yang He, Yu Cheng, Suleman Saeed, and Jihong Zhu

***Abstract*—To deal with the single-phase open-circuited fault, an enhanced fault-tolerant model predictive current control with continued modulation is proposed in this article. This method includes reconstructing the postfault vector distribution and adopting a multistep vector selection method. In the reconstruction procedure, the transition vectors are generating to realize standard pulsewidth modulation waveforms. Then, the unreachable area can be filled by creating new synthetic vectors. Finally, the vectors with oversized amplitudes are optimized by using null vectors. In order to cover the full modulation area, a multistep vector selection method is used to determine the phase angle and amplitude of the optimal vector. The phase angle can be determined by defining two cost functions and adopting duty cycle modulation technology. The amplitude of the optimal vector can be optimized by utilizing the duty cycle modulation technology again. The oscillation, due to the back electromotive force, is compensated in each step. A thorough experimental evaluation has been conducted to confirm the effectiveness and superiority of the proposed fault-tolerant method.**

***Index Terms*—Back electromotive force (EMF) compensation, continued modulation, fault-tolerant control, five-phase motor, model predictive control, multistep vector selection, open-circuited.**

I. Introduction

MULTIPHASE motor drives have attracted significant attention due to the development of control theory and power electronics. Compared with their three-phase counterparts, the multiphase motors have extra control freedom, which can be utilized to realize fault-tolerant control without additional hardware circuit and downtime maintenance. So, the fault-tolerant control for multiphase drives has been studied widely [1]–[4].

Among all types of faults, the open-circuited failures of motor phases are the most common scenarios. To deal with this faulty situation, calculating the fault-tolerant current references is one kind of a commonly used fault-tolerant strategy. In these methods, the decoupling matrix in the postfault condition is the same as that of the normal situation. In order to track the fault-tolerant current references, hysteresis current regulator [5], [6], PI regulator [7], [8], and dual-PI regulator [9], [10] were investigated. However, the performance of current regulator affects the fault-tolerant control. For example, the use of the hysteresis current regulator leads to unfixed switching frequency. The limited bandwidth of the PI regulator cannot track the fault-tolerant current references effectively. Another fault-tolerant strategy is utilizing a reduced decoupling matrix. In this strategy, the fault-tolerant controls are not dependent on designing the current regulator. The fault-tolerant controls in the synchronous reference frame with a PI regulator were investigated in [11] and [12]. In these methods, the feedforward control and the repeated tuning process were necessary. The fault-tolerant direct torque control (DTC) schemes with a nonorthogonal reduced decoupling matrix were discussed in [13] and [14]. In this method, a modified lookup table was used in the postfault situation, which includes ten virtual voltage vectors. However, the fixed amplitudes of the virtual voltage vectors were the main drawback of this method. A pulsewidth modulation (PWM) based fault-tolerant DTC control was introduced in [15], where the virtual stator flux was used to achieve circular trajectories of current and rotating magnetomotive force. However, a feedforward voltage was necessary, which leads to extra complexity.

Recently, the finite control set model predictive control (FCS-MPC) was adopted to deal with the faulty situation due to the merits of high bandwidth, easy tuning process, and intuitive concept [16]–[19]. A single-vector fault-tolerant finite control set model predictive current control (FCS-MPCC) was introduced in [16]. In this method, the x-axis component was abandoned, and the y-axis component can be controlled to realize fault-tolerant control. However, it is difficult to improve the fault-tolerant operation performance due to the discrete candidate vectors. In [17], the duty cycle modulation technology was combined with fault-tolerant FCS-MPCC. However, all the

Manuscript received May 21, 2020; revised July 5, 2020; accepted August 11, 2020. Date of publication August 25, 2020; date of current version October 30, 2020. This work was supported in part by the National Natural Science Foundation of China under Grant 51777090, in part by the Key Research and Development Program of Jiangsu Province under Grant BE2018107, and in part by the Priority Academic Program Development of Jiangsu Higher Education Institutions. Recommended for publication by Associate Editor D. G. Xu. *(Corresponding author: Wenxiang Zhao.)*

Tao Tao, Wenxiang Zhao, Yang He, Yu Cheng, and Suleman Saeed are with the School of Electrical and Information Engineering, Jiangsu University, Zhenjiang 212013, China (e-mail: 15862935596@163.com; zwx@ujs.edu.cn; heyang@ujs.edu.cn; 3130501041@stmail.ujs.edu.cn; suleman.saeed.r@outlook.com).

Jihong Zhu is with the Department of Precision Instrument, Tsinghua University, Beijing 100084, China (e-mail: jhzhu@tsinghua.edu.cn).

Color versions of one or more of the figures in this article are available online at https://ieeexplore.ieee.org.

Digital Object Identifier 10.1109/TPEL.2020.3018302

available vectors are necessary to be evaluated by a predefined cost function. This conventional optimization process leads to a huge computational burden. In [18], the fault-tolerant virtual voltage vectors were employed as the control set. However, the fixed and finite candidate virtual vectors inevitably lead to deteriorated operation performance. In [19], a fault-tolerant model predictive torque control with a space vector modulation was proposed. However, the harmonic currents were added into the cost function, which leads to the difficult tuning process. For the fault-tolerant FCS-MPC (FT-MPC), the discontinued modulation area is the main reason for deteriorated operation performance.

The FCS-MPC with continued modulation was studied in [19]–[22]. Typically, two duty cycles were necessary to determine the phase angle and optimal amplitude. However, the overflow of the two duty cycles was often neglected [19], [20]. A five-phase FCS-MPCC with continued modulation was discussed in [22], where the vectors with harmonic free were employed as the control set. The other kind of MPC with continued modulation is the continuous control set MPC. This strategy computes a continuous control signal and uses a modulator to generate the desired output voltage [23]. Obviously, the modulator is necessary. Also, the complex formulation of the MPC problem is the main problem of this strategy [24]. However, all the mentioned schemes were proposed for normal operation. In the faulty situation, the postfault vector distribution becomes irregular. Specifically, the implementation of FCS-MPC can be less efficient. The reason is that the candidate vectors have different amplitudes and irregular distribution. Also, the multivector combination becomes complex. This is because it is necessary to consider the harmonic components and standard PWM waveforms simultaneously. In addition, the disturbance due to the back electromotive force (EMF) of the faulty phase should be considered.

In this article, an FT-MPC with continued modulation will be proposed. A reconstructed vector distribution is introduced in which the PWM generation and implementation of FCS-MPCC are considered. In addition, a multistep vector selection method is used to cover the full modulation area. Moreover, the oscillation generated from the back EMF of the faulty phase is considered in the vector selection procedure. The rest of the article is organized as follows. Section II briefly describes the predictive model of the motor with an open-circuited fault. Two conventional FT-MPCs are discussed in Section III. Based on the two conventional FT-MPCs, the proposed method is presented in Section IV. Section V provides the experimental results to show and discuss the performance of the proposed fault-tolerant control. Finally, the conclusion is presented in Section VI.

II. Predictive Model of Postfault Motor

The five-phase permanent magnet (PM) motor is driven by using a five-phase two-level voltage-source inverter. In normal situations, there are 30 active vectors and 2 null vectors. Assuming an open-circuited fault occurs, the available vectors reduced from 32 to 16. A reduced decoupling matrix is used in this article to ensure the same discrete equation before and after the fault.

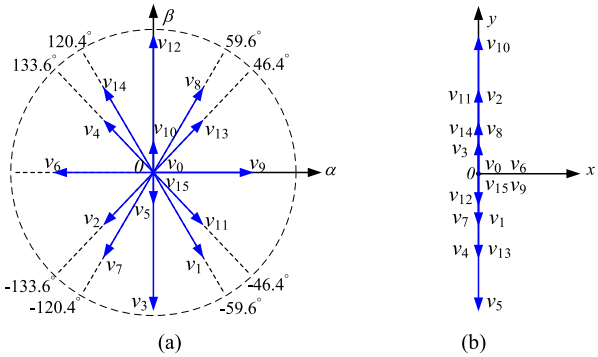

Fig. 1. Postfault voltage vectors. (a) α–β space. (b) y-axis.

This reduced decoupling matrix can be expressed as

$$T_{\text{postfault}} = \frac{2}{5}\begin{bmatrix} \cos\gamma - 1 & \cos2\gamma - 1 & \cos3\gamma - 1 & \cos4\gamma - 1 \\ \sin\gamma & \sin2\gamma & \sin3\gamma & \sin4\gamma \\ \sin2\gamma & \sin4\gamma & \sin6\gamma & \sin8\gamma \\ 1 & 1 & 1 & 1 \end{bmatrix} \tag{1}$$

where $\gamma = 2\pi/5$. The rotational transformation (2) can be used to transform α–β space components into the d–q space

$$D(\theta_r) = \begin{bmatrix} \cos\theta_r & \sin\theta_r & 0 & 0 \\ -\sin\theta_r & \cos\theta_r & 0 & 0 \\ 0 & 0 & 1 & 0 \\ 0 & 0 & 0 & 1 \end{bmatrix} \tag{2}$$

where θ_r is the rotor position. According to the articles presented in [14] and [18], the current predictive model under open-circuited situation can be expressed as

$$i_s(k+1) = i_s(k) + \frac{T_s}{L_s}(u_s - r_s i_s(k) + e) \tag{3}$$

where

$$i_s = [i_d \quad i_q \quad i_y]^T$$

$$\frac{1}{L_s} = \left[\frac{1}{L_d} \quad \frac{1}{L_q} \quad \frac{1}{L_{ls}}\right]^T$$

$$e = [\omega_e L_q i_q \quad -\omega_e(L_d i_d + \psi_f) \quad 0]^T$$

u_s is the control set, which includes 16 vectors; r_s is the stator resistance; and L_d and L_q are the d–q axis inductances, respectively; i_d and i_q are the d–q axis currents, respectively; i_y is the current of the y-axis; L_{ls} is the leakage inductance; ω_e is the angular velocity; T_s is the sampling period; and ψ_f is the PM flux linkage.

III. Existing FT-MPCs

Based on (1)–(3), two existing fault-tolerant controls are discussed in this section. The drawbacks of the two controls are analyzed.

A. Duty Cycle Modulation Based Fault-Tolerant Control

According to (1), the postfault vector distribution can be depicted in Fig. 1, which includes 14 active vectors and 2 null

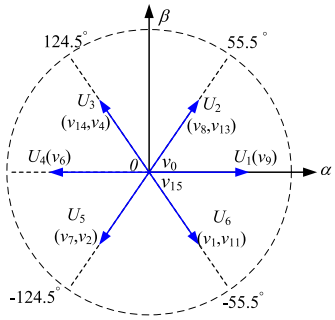

Fig. 2. Postfault virtual voltage vectors.

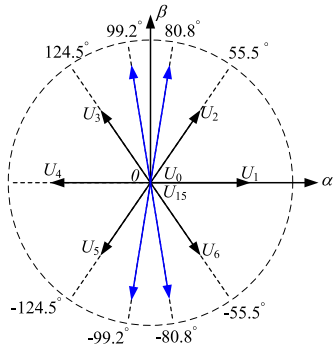

Fig. 3. Postfault vector distribution with transition vectors.

vectors. The amplitude of v_9, v_{13}, v_8, and v_{12} is 0.447, 0.325, 0.441, and 0.616, respectively. The corresponding vectors in other sectors have the same amplitudes. In one control period, by allocating execution time to the null vectors, the amplitudes of the active vectors can be optimized. This means the modulation area can be extended from 16 discrete points to 14 lines. In this fault-tolerant control, the cost function can be expressed as

$$\boldsymbol{J} = (i_d^* - i_d(k+1))^2 + (i_q^* - i_q(k+1))^2 + (i_y^* - i_y(k+1))^2. \quad (4)$$

The minimum copper loss can be realized by setting $i_y^* = 0$. However, as shown in Fig. 1, the combinations of one active vector and the null vector lead to unsatisfied restraint of harmonic currents. Considering the irregularity vector distribution, it is difficult to realize continued modulation and restrain the y-axis currents simultaneously.

B. Virtual Voltage Vectors Based Fault-Tolerant Control

The virtual voltage vectors based fault-tolerant control was introduced in [18]. This method reduces the extra consideration of harmonic components by generating fault-tolerant virtual voltage vectors. The fault-tolerant virtual voltage vectors are shown in Fig. 2. It should be noted that U_2, U_3, U_5, and U_6 are generated by using two basic vectors of Fig. 1. The duration is fixed to 0.618. U_1 and U_4 include one basic vector. By using this method, the harmonic components can be eliminated. So, the y-axis components in (3) can be abandoned, and the cost function can be expressed as

$$\boldsymbol{J} = (i_d^* - i_d(k+1))^2 + (i_q^* - i_q(k+1))^2. \quad (5)$$

In this method, the candidate vectors with fixed amplitude inevitably lead to rough control. Also, finite vectors are the real challenge to further improve the operational performance. Extending the control to incorporate more candidate vectors can solve this problem [25]. However, in the faulty situation, the standard PWM waveforms may not be generated by using the adjacent vectors.

IV. Proposed Fault-Tolerant Control

The implementation of the proposed fault-tolerant control can be summarized as the following. First, the distribution of the postfault vector is reconstructed. Second, a multistep vector selection method with back EMF compensation is utilized to cover the full modulation area.

A. Reconstruction of Postfault Vector Distribution

A reconstructed vector distribution is proposed, which is the premise of realizing continued modulation in the faulty situation. This reconstructed vector distribution is the extension of the virtual voltage vectors in Fig. 2. The implementation of FCS-MPCC and standard PWM waveforms is considered.

1) Generating Transition Vectors: In order to realize continued modulation, the adjacent two vectors are often utilized. So, the switching sequence of the adjacent two vectors should be taken into consideration. However, U_2 (v_8[1000], v_{13}[1101]) and U_3 (v_{14}[1110], v_4[0100]) in Fig. 2 cannot generate standard PWM waveforms. This is because the switching states of v_8 and v_4 are conflicting. In this article, the transition vectors are synthesized to solve this problem. According to Fig. 1(a) and (b), v_{12}(1100) can be utilized to generate the transition vectors. Specifically, the transition vectors between U_2 and U_3 can be synthesized by using $0.618v_{12}+0.382v_8$ and $0.618v_{12}+0.382v_{14}$. Also, v_3 can be utilized to generate the transition vectors of U_5 and U_6, and the synthesis principle is $0.618v_3+0.382v_7$ and $0.618v_3+0.382v_1$. All four transition vectors are shown in Fig. 3 (blue lines), which preserve harmonics-free.

By generating the transition vector, the sector between U_2 and U_3 can be partitioned into three parts. The adjacent two vectors of each section can generate standard PWM waveforms.

2) Extend the Control Set: According to Fig. 3, the unreachable area between U_1 and U_2 ($[U_3, U_4]$, $[U_4, U_5]$, $[U_6, U_1]$) is too large. This means if the desired vector is in these unreachable areas, the control error might be unaccepted. Also, the vector selection might be inaccurate. This is because the amplitude and phase angle of the candidate vectors affect the vector determination. Generating new candidate vectors to extend the control set can solve this problem. The extended control set is shown in Fig. 4, where four synthetic vectors (blue lines) are generated by using the adjacent two vectors. In this place, the duration of the adjacent two vectors ($[U_1, U_2]$, $[U_3, U_4]$, $[U_4, U_5]$, and $[U_6, U_1]$) is fixed to 0.5.

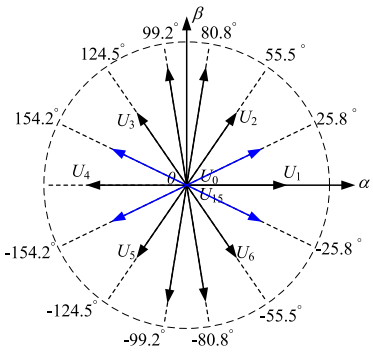

Fig. 4. Postfault vector distribution with an extended control set.

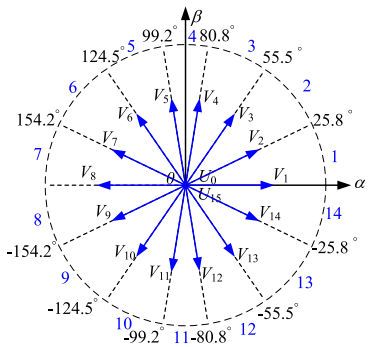

Fig. 5. Postfault voltage vector after restructuring.

TABLE I
DETAILED VECTOR RECONSTRUCTION

V_i	v_m	v_n	d
V_1	v_9	v_9	0.9
V_2	$0.5\times v_9+0.5\times v_{13}$	$0.5\times v_9+0.5\times v_8$	1
V_3	v_{13}	v_8	1
V_4	v_8	v_{12}	0.75
V_5	v_{14}	v_{12}	0.75
V_6	v_4	v_{14}	1
V_7	$0.5\times v_4+0.5\times v_6$	$0.5\times v_{14}+0.5\times v_6$	1
V_8	v_6	v_6	0.9
V_9	$0.5\times v_2+0.5\times v_6$	$0.5\times v_7+0.5\times v_6$	1
V_{10}	v_2	v_7	1
V_{11}	v_7	v_3	0.75
V_{12}	v_1	v_3	0.75
V_{13}	v_{11}	v_1	1
V_{14}	$0.5\times v_9+0.5\times v_{11}$	$0.5\times v_9+0.5\times v_1$	1

3) Amplitude Optimization: As shown in Fig 4, the amplitudes of the four transition vectors, U_1 and U_4 are oversized. This is not beneficial for the implementation of FCS-MPC. So, the third step is to optimize the amplitude by utilizing the null vector. In order to reduce the complexity, the duration of the four transition vectors is fixed to 0.75, and the duration of U_1 and U_4 is set to 0.9. It should be noted that the reduction of these oversized amplitudes shortens the modulation area. However, this amplitude optimization improves the accuracy of vector selection. This is because these vectors with oversized amplitudes are difficult to minimize the cost function, which means the available vectors are reduced.

Generally, the principle of vector reconstruction can be expressed as

$$V_i(v_m, v_n, d, v_0) = d(0.382v_m + 0.618v_n)+(1-d)v_0 \quad (6)$$

where 0.618 and 0.382 are used to ensure harmonics-free; d is used to optimize the oversized amplitude; and $v_{m,n}$ and v_0 are the active vectors and null vectors, respectively, as depicted in Fig. 1. The detailed vector combinations are listed in Table I.

The reconstructed vector distribution is depicted in Fig. 5. Obviously, the new vector distribution is near regular, which is suitable for FCS-MPCC. Also, the standard PWM waveforms can be generated by using the adjacent two vectors. So, the premise of the proposed fault-tolerant control with continued modulation can be realized.

B. Back EMF Compensation

The above analysis is based on the postfault switching state. When an open-circuit fault occurs, the current of the faulty phase becomes zero, and its voltage is given by its back EMF. So, the back EMF of the faulty phase should be incorporated by the voltage equation. Assuming an open-circuited fault occurs in phase a, the relationship of the voltage equation and drive signals should be modified as

$$\begin{bmatrix} u_\alpha \\ u_\beta \\ u_y \\ u_0 \end{bmatrix} = T_{\text{postfault}} \left(\frac{u_{\text{dc}}}{4} \begin{bmatrix} 3 & -1 & -1 & -1 \\ -1 & 3 & -1 & -1 \\ -1 & -1 & 3 & -1 \\ -1 & -1 & -1 & 3 \end{bmatrix} \begin{bmatrix} g_b \\ g_c \\ g_d \\ g_e \end{bmatrix} - \frac{\text{emf}_a}{4} \begin{bmatrix} 1 \\ 1 \\ 1 \\ 1 \end{bmatrix} \right) \quad (7)$$

where g_i ($i = b, c, d, e$) are the drive signals; $u_{\alpha,\beta}$ are the voltages in α–β space; emf_a is the back EMF of phase a; u_y is the y-axis voltage; and u_0 is the zero-sequence voltage.

Equation (7) includes an uncontrolled oscillation caused by the back EMF of phase a [16], which is not exist in the normal situation. Obviously, this oscillation affects the vector selection. In the proposed method, this back EMF is incorporated into the control set. This means this oscillation has been considered by the vector selection procedure.

C. Determination of Optimal Vector

For the conventional FCS-MPC, the finite and discontinued candidate vectors are the main reasons for deteriorated operational performance. In the proposed method, a multistep vector selection method is used to determine the phase angle and amplitude of the optimal vector. The multistep vector selection method includes two optimization problems in which the basic principle of classic FCS-MPC is utilized. Also, the duty cycle modulation technology is adopted twice. The block diagram of the proposed fault-tolerant control is shown in Fig. 6. The red

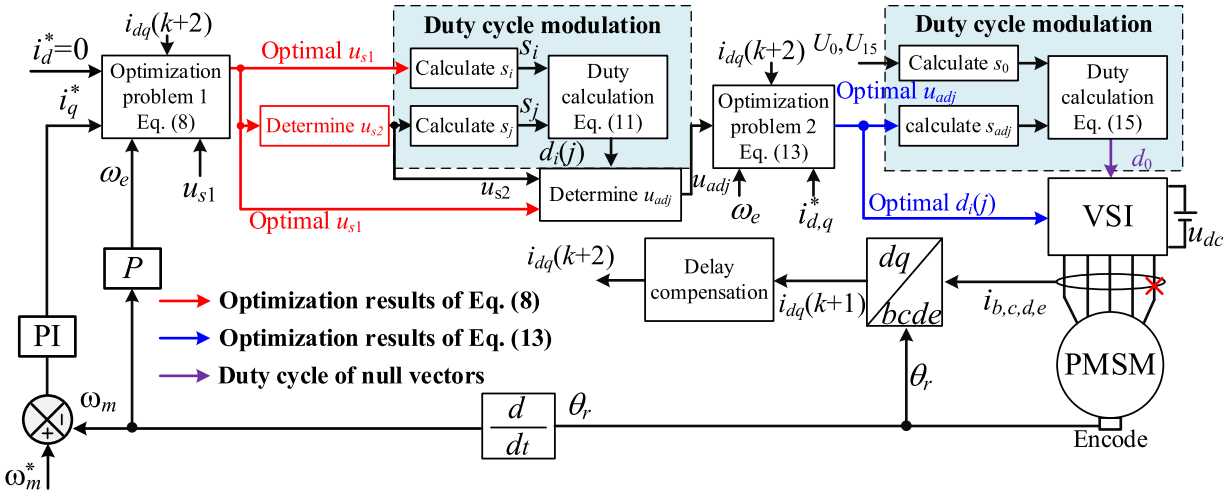

Fig. 6. Block diagram of the proposed fault-tolerant control.

lines in Fig. 6 are the optimization results of (8), which include choosing the first optimal vector and determining the second control set. The blue lines represent the optimization results of (13). In this step, the optimal combination of the adjacent two vectors is chosen. The duty cycle of the null vectors can be determined based on the current work condition. The calculated two duty cycles will be applied to the inverter directly.

1) Phase Angle Determination: The determination of the phase angle includes two steps. In the first step, a control set is defined, which includes seven nonadjacent vectors of Fig. 5. These vectors are evaluated by defining optimization problem 1, which can be expressed as

$$\begin{aligned} &\min J_1 = \text{norm}(i_{dq}^* - i_{dq}(k+1))^2 \\ &\text{s.t. } i_{dq}(k+1) = i_{dq}(k) + \frac{T_s}{L_{dq}}(u_{s1} - r_s i_{dq}(k) + e_{dq}) \\ &u_{s1} \in \left\{ \begin{matrix} V_{1\_dq}, V_{3\_dq}, V_{5\_dq}, V_{7\_dq}, \\ V_{9\_dq}, V_{11\_dq}, V_{13\_dq} \end{matrix} \right\} - \frac{\text{emf}_{a\_dq}}{4} \end{aligned} \tag{8}$$

where

$$\begin{aligned} i_{dq}(k+1) &= [i_d(k+1) \quad i_q(k+1)]^T \\ e_{dq} &= [\omega L_q i_q \quad -\omega(L_d i_d + \psi_f)]^T \\ i_{dq}^* &= [i_d^* \quad i_q^*]^T \\ \frac{1}{L_{dq}} &= \left[\frac{1}{L_d} \quad \frac{1}{L_q}\right]^T \end{aligned}$$

and emf_{a_dq} is the back EMF of phase a in the d–q coordinate system; and V_{i_dq} ($i = 1, 2, 3, \ldots, 14$) are the candidate vectors of Fig. 5 in the d–q coordinate system. It should be noted that the y-axis component is eliminated in the predictive model due to the vectors with harmonic free.

Assuming V_1 is selected from the optimization problem 1, then the adjacent two vectors of V_1 can be determined. The next step is to determine the optimal combination by using a duty cycle modulation technology. In this article, the deadbeat principle of the d–q axis currents is adopted to calculate the duty cycle. This principle can be expressed as

$$i_{dq}(k+1) = i_{dq}(k) + s_j(T_s - T_i) + s_i T_i = i_{dq}^* \tag{9}$$

where

$$\begin{aligned} s_i &= \left.\frac{di_s}{dt}\right|_{u_{s1}=V_{1\_dq}-\frac{\text{emf}_{a\_dq}}{4}} \\ s_j &= \left.\frac{di_s}{dt}\right|_{u_{s2}=\{V_{2\_dq},V_{14\_dq}\}-\frac{\text{emf}_{a\_dq}}{4}} \end{aligned}$$

and T_i is the execution time of u_{s1}.

Equation (9) is a function of T_i by solving

$$\frac{\partial((i_d^* - i_d(k+1))^2 + (i_q^* - i_q(k+1))^2)}{\partial T_i} = 0. \tag{10}$$

The duty cycles and execution time of u_{s2} can be calculated as

$$d_i(j) = \frac{\text{dot}((i_{dq}^* - i_{dq}(k+1) - s_j T_s), (s_j - s_i))}{T_s \times (s_j - s_i)^2} \tag{11}$$

$$(T_s - T_i) = d_i(j) \times T_s. \tag{12}$$

Then, two synthetic vectors are evaluated by defining the optimization problem 2, which can be expressed as

$$\begin{aligned} &\min J_2 = \text{norm}(i_{dq}^* - i_{dq}(k+1))^2 \\ &\text{s.t. } i_{dq}(k+1) = i_{dq}(k) + \frac{T_s}{L_{dq}}(u_{\text{adj}} - r_s i_{dq}(k) + e_{dq}) \\ &u_{\text{adj}} \\ &\in \left\{ d_1(2)\left(V_{2\_dq} - \frac{\text{emf}_{a\_dq}}{4}\right) + (1 - d_1(2))\left(V_{1\_dq} - \frac{\text{emf}_{a\_dq}}{4}\right), \right. \\ &\left. d_1(14)\left(V_{14\_dq} - \frac{\text{emf}_{a\_dq}}{4}\right) + (1 - d_1(14))\left(V_{1\_dq} - \frac{\text{emf}_{a\_dq}}{4}\right) \right\}. \end{aligned} \tag{13}$$

According to (13), the duty cycle and the corresponding vector are evaluated by J_2, simultaneously. Assuming $d_1(2)$ and V_2 are determined in the optimization problem 2. In this situation, the synthetic vector can be expressed as

$$\begin{aligned} u_{\text{adj}} = {} & d_1(2)\left(V_{2\_dq} - \frac{\text{emf}_{a\_dq}}{4}\right) \\ & + (1 - d_1(2))\left(V_{1\_dq} - \frac{\text{emf}_{a\_dq}}{4}\right). \end{aligned} \tag{14}$$

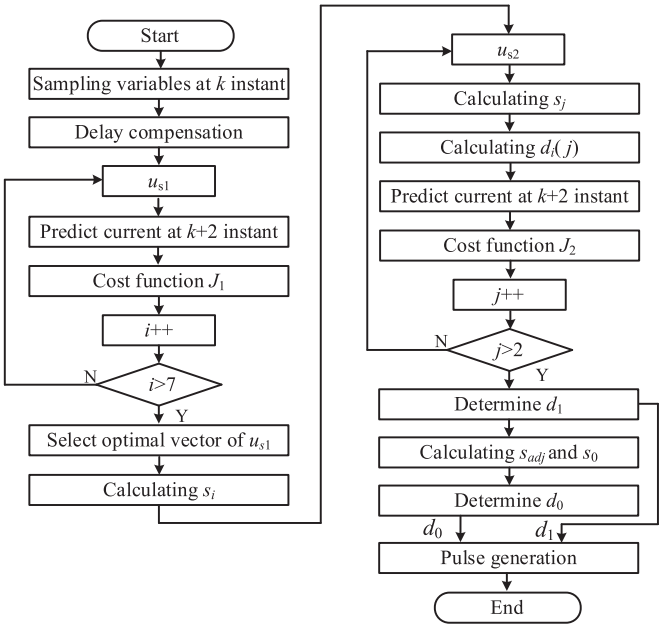

Fig. 7. Flowchart of the proposed method.

2) Amplitude Determination: Obviously, u_{adj} has a fixed amplitude, which leads to rough control. By allocating execution time to the two null vectors, the amplitude of u_{adj} can be optimized. In this situation, the duty cycle modulation technology is adopted again. Similar to (10) and (11), the duty cycle of the null vectors can be expressed as

$$d_0 = \frac{\mathrm{dot}((i^*_{dq} - i_{dq}(k) - s_{\mathrm{adj}}T_s), (s_0 - s_{\mathrm{adj}}))}{T_s \times (s_0 - s_{\mathrm{adj}})^2} \tag{15}$$

where

$$s_{\mathrm{adj}} = \left.\frac{di_s}{dt}\right|_{u_s = u_{\mathrm{adj}}} \quad s_0 = \left.\frac{di_s}{dt}\right|_{u_s = U_0 \mathrm{or} U_{15}}.$$

After the determination of d_0, the optimal synthetic vector can be expressed as

$$u_{\mathrm{opt}} = (1 - d_0) \times u_{\mathrm{adj}}. \tag{16}$$

D. Overall Control Scheme

The flowchart of the proposed method is depicted in Fig. 7. According to Fig. 7, the phase angle and amplitude can be determined by using the multistep vector selection method, which might be not easy than using a modulator. However, the classic principle of FCS-MPCC is adopted twice, which means the proposed method has intuitive formulation. Also, the proposed method preserves the merits of classic FCS-MPCC, which include easy inclusion of nonlinear constraints and easy tuning process.

For the multistep vector selection method, there are seven vectors evaluated in the optimization problem 1, and two vectors are assessed in the optimization problem 2. Obviously, not all the candidate vectors are evaluated in one control period, which means the computational burden can be reduced. The selected

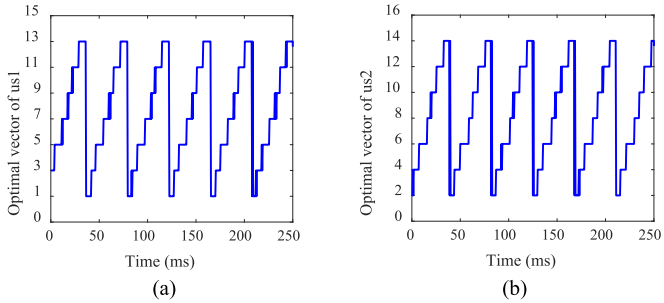

Fig. 8. Optimal vectors. (a) Optimization vector of u_{s1}. (b) Optimization vector of u_{s2}.

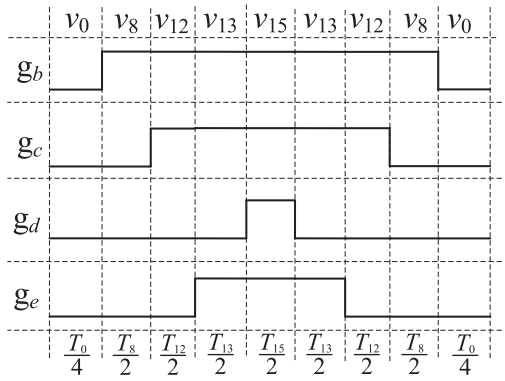

Fig. 9. Switching sequences of reconstructed sector 3.

vectors of optimization problem 1 and optimization problem 2 are shown in Fig. 8. According to the results, all the candidate vectors can be chosen. This means the vector selection can determine the optimal vector without evaluating all the candidate vectors.

The switching sequences of the reconstructed sector 3 are shown in Fig. 9, where the drive signal of the faulty phase is OFF. In this situation, V_3 is determined in the first optimization problem 1, and V_4 is selected in the optimization problem 2. As discussed earlier, the standard PWM waveforms can be generated, which is easy to implement by digital signal processing.

The executing time of each basic vector in Fig. 9 can be obtained as

$$T_0 = T_{15} = d_0 T_s + (1 - d_0) d_3(4) \times 0.25 T_s$$

$$T_{13} = (1 - d_0)(1 - d_3(4)) \times 0.382 T_s$$

$$T_{12} = 0.75(1 - d_0) d_3(4) \times 0.618 T_s$$

$$T_8 = (1 - d_0)(1 - d_3(4)) \times 0.618 T_s + 0.75(1 - d_0) d_3(4) \times 0.382 T_s.$$

It should be noted that the vector selection method is similar to that of the article presented in [22]. However, in the fault-tolerant control situation, the back EMF of the faulty phase should be considered in the multistep vector selection procedure. The synthesized vector of (16) is the result of the multistep vector selection procedure, where the back EMF of the faulty phase is considered. The simulation results of the stator voltage with

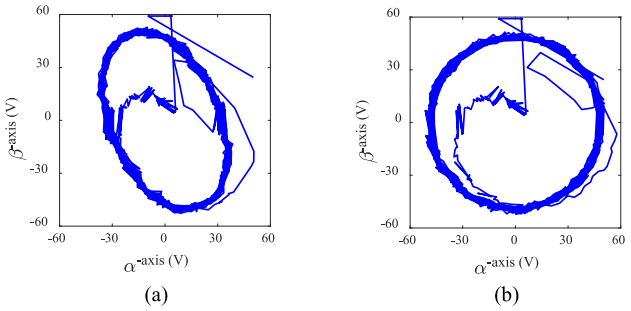

Fig. 10. Stator voltage. (a) Without back EMF compensation. (b) With back EMF compensation.

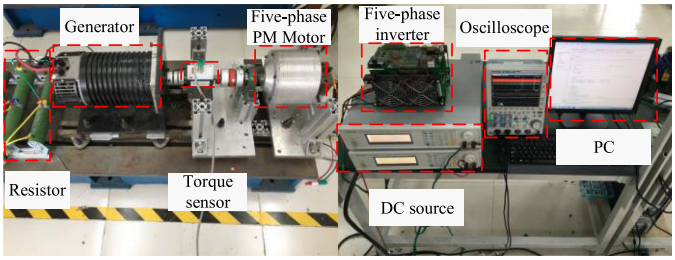

Fig. 11. Experimental platform.

and without the back EMF compensation are shown in Fig. 10. As shown in Fig. 10(a), the stator voltage without the back EMF compensation is elliptical. The reason is the oscillation generated from the back EMF of the faulty phase. When the back EMF of the faulty phase is considered in (8), (9), and (13), the stator voltage becomes circular, which is shown in Fig. 10(b). This means the back EMF compensation is useful.

V. Experimental Results

A. Experimental Platform

An experimental platform is established to verify the superiorities of the proposed fault-tolerant control, which is shown in Fig. 11. A DSP TMS320F28377 is used to implement the algorithm. The sampling frequency is set to 20 kHz. A dc generator is mechanically coupled to a five-phase PM Vernier machine to provide the electric load. This Vernier machine is designed for the direct-drive application. A solid-state relay is adopted to simulate the open-circuited fault, which is controlled by the DSP.

B. Steady-State Performance

The experiments of two conventional FT-MPCs and a continued FCS-MPCC for a normal situation are conducted. The brief introduction of the three methods is as follows.

Continued FCS-MPCC [22]: This method introduces an FCS-MPCC with continued modulation for normal operation. There are four active vectors and two null vectors applied in one control period.

FT-MPC1: The candidate vectors, as shown in Fig. 4, are employed as the control set, which includes 14 active vectors

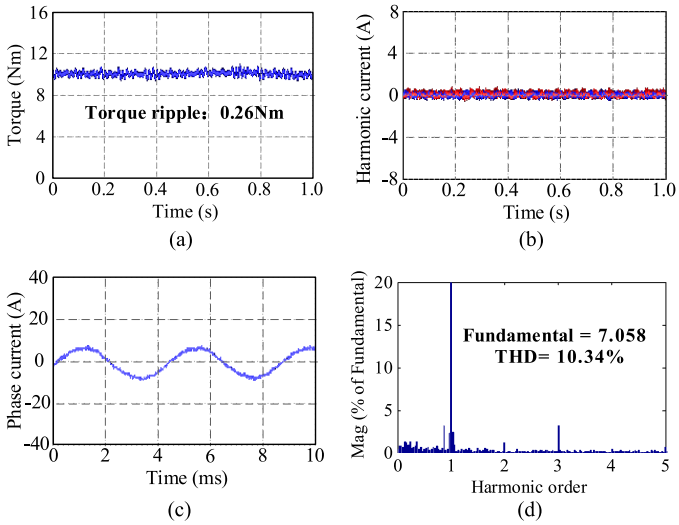

Fig. 12. Experimental results of FCS-MPC with continued modulation for normal operation [22]. (a) Torque. (b) *xy*-axis current. (c) Phase current. (d) Total harmonic distortion (THD) analysis of phase current.

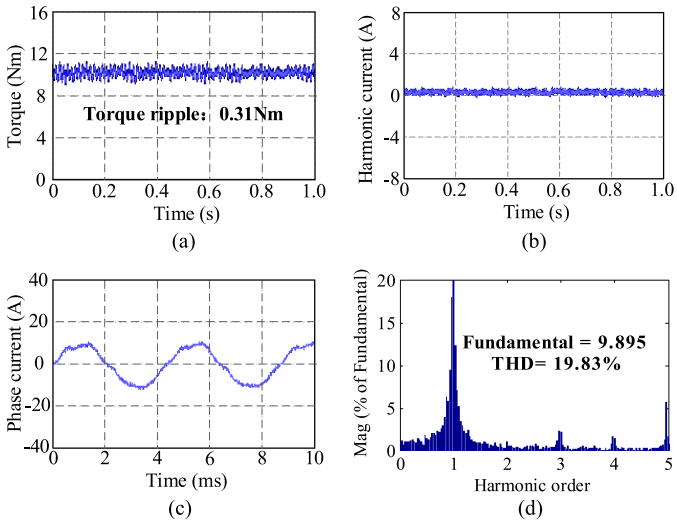

Fig. 13. Experimental results of FT-MPC1. (a) Torque. (b) *y*-axis current. (c) Phase current. (d) THD analysis of phase current.

and 2 null vectors (the oversized amplitudes are not optimized). The vector selection method introduced in Section IV is utilized by this method.

FT-MPC2: The reconstructed vector distribution, as shown in Fig. 5, is employed as the control set. By using the duty cycle modulation technology, the 14 candidate vectors with optimal amplitude are evaluated by defining optimization problem 1. The modulation area of this method is discontinued.

Figs. 12–15 compare the above three methods and the proposed method. In the experiments, the speed reference is set to 450 r/min, and the load torque is 10 N·m. Fig. 12 presents the experimental results of the method introduced in [22]. Obviously, the steady-state performance is excellent. This is because the adjacent four vectors are applied in one control period, which

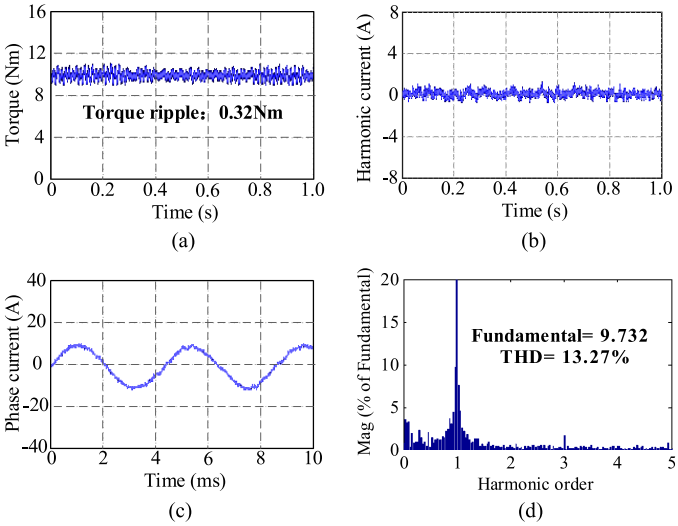

Fig. 14. Experimental results of FT-MPC2. (a) Torque. (b) y-axis current. (c) Phase current. (d) THD analysis of phase current.

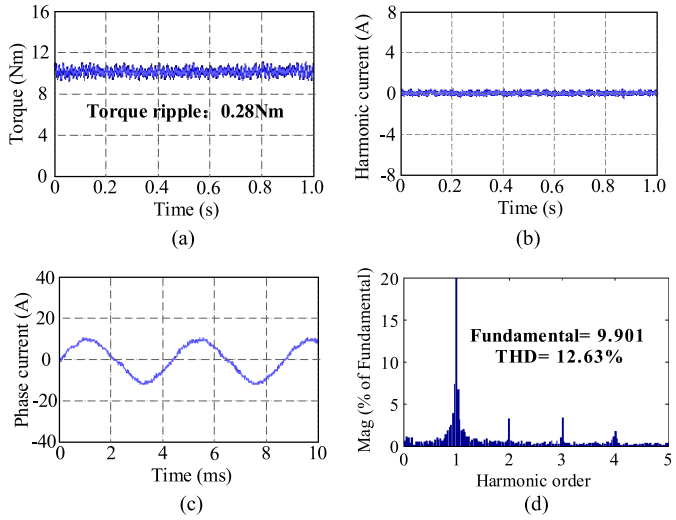

Fig. 15. Experimental results of the proposed fault-tolerant control. (a) Torque. (b) y-axis current. (c) Phase current. (d) THD analysis of phase current.

is the same as that of the conventional five-phase space vector modulation.

Fig. 13 shows the experimental results of FT-MPC1. The torque ripples and phase current amplitude become larger due to the open-circuited fault. The torque ripple, as illustrated in Fig. 13(a), is 0.31 N·m. The harmonic currents in Fig. 13(b) can be restrained well. The phase current in Fig. 13(c) is distorted severely. The total harmonic distortion (THD) value is 19.83%, where the main harmonic components are third-, fourth-, and fifth-order harmonics. According to the result, even with a continued modulation, the irregular vector distribution might lead to deteriorated operation performance. The reason is that the oversized candidate vectors affect the vector selection.

The experimental results of FT-MPC2 are shown in Fig. 14. The torque ripple of this method is slightly higher than that of

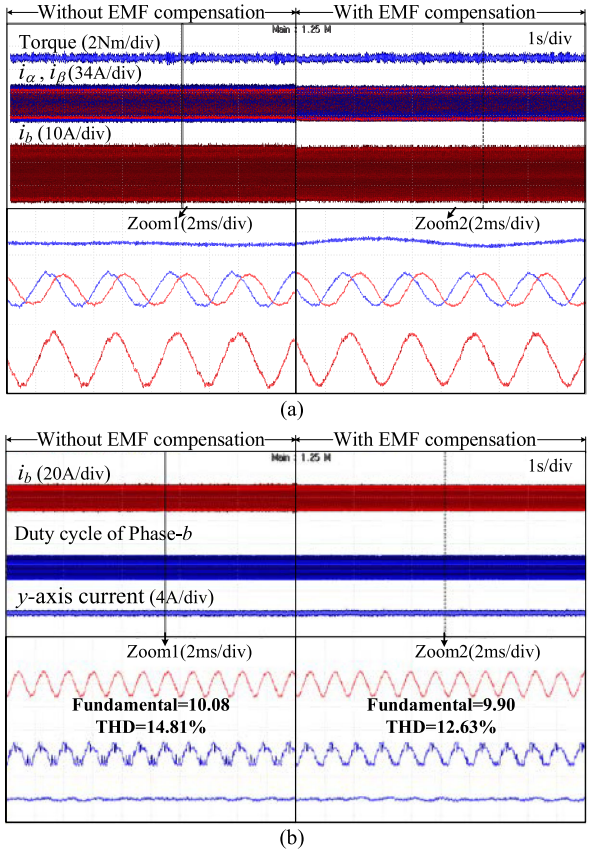

Fig. 16. Steady-state performance with and without the back EMF compensation. (a) Phase current, torque, and $\alpha\beta$-axis currents. (b) Phase current, duty cycle, and harmonic currents.

the FT-MPC1. Compared with Fig. 13(b), the harmonic of this method cannot be restrained well. This is because the optimal vector has a fixed phase angle, and fewer vectors are applied in one control period. The phase current in Fig. 14(c) is more sinusoidal than that in Fig. 13(c). The THD value in Fig. 14(d) is 13.27%, which is lower than that of the FT-MPC1. This experimental result demonstrates that vector reconstruction is effective in improving the quality of the phase current. However, the harmonic currents cannot be restrained well due to the discontinued modulation.

Fig. 15 shows the experimental results of the proposed method. The torque ripple is 0.28 N·m, which is lower than that of the two existing FT-MPCs. The phase current in Fig. 15(c) is closer to standard sinusoidal waveforms. As depicted in Fig. 15(d), the fourth- and fifth-order harmonics are eliminated. So, the THD value of the proposed method is lower than that of the two FT-MPCs. Compared with the FT-MPC2 with discontinued modulation, a better restrain of harmonic current can be obtained by adopting the multistep vector selection method. The reason is that the optimal vector has an optimal phase angle and amplitude. Also, combined with the results of FT-MPC1, the results of Fig. 15 verify that the reconstructed vector distribution is effective in improving operational performance further.

Fig. 16 shows the experimental results of the proposed fault-tolerant control with and without the back EMF compensation.

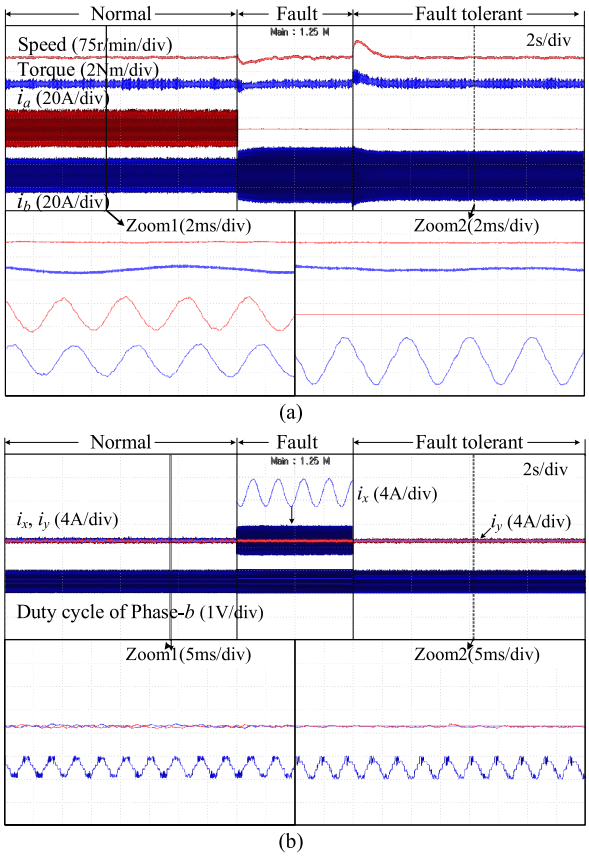

Fig. 17. Switching process of the proposed fault-tolerant control. (a) Torque, speed, and phase currents. (b) Harmonic currents and duty cycle.

In this experiment, the load torque is 10 N·m, and the reference speed is set to 450 r/min.

According to Fig. 16(a), the proposed method without back EMF compensation leads to asymmetrical $\alpha\beta$-axis currents, where the amplitudes are different. When the back EMF is considered, the amplitudes of $\alpha\beta$-axis currents become equal. Also, the amplitude of the phase current is slightly lower than that of the control without back EMF compensation. The results of Fig. 16(b) show that the back EMF compensation has a little affect on the harmonic current. Also, the current distortion can be improved. The duty cycle in Fig. 16(b) indicates when the oscillation is considered, the calculated duty cycle is more accurate. As a result, by using the vector selection method with back EMF compensation, the oscillation from the faulty phase can be eliminated.

C. Online Switching Experiments

Fig. 17 shows the experimental results of the online switching process. In this experiment, the five-phase motor is operated in a normal situation for a few seconds. Then, phase a is disconnected by using a solid-state relay. After 4 s, the proposed FT-MPC is implemented. The waveforms of actual speed, phase currents, harmonic currents, duty cycle, and torque are recorded.

It can be seen from Fig. 17(a) that at normal operation, the torque and speed are smooth and the harmonic currents can be restrained well. When an open-circuit fault occurs, the current of phase a becomes zero, the current amplitude of the healthy phase is increased, and the speed ripples become large. In this condition, the x-axis current in Fig. 17(b) becomes sinusoidal, which is out of control. After the implementation of the proposed fault-tolerant control, the current amplitude of the healthy phase can be reduced, and the reduction of speed ripples in the fault-tolerant operation is visible, which is nearly the same as that of the normal operation. Meanwhile, the x-axis component is eliminated due to the reduced decoupling matrix, and the y-axis current can be restrained well. Moreover, the waveform of the duty cycle varies in the sinusoidal form, which means the duty cycle calculation method is feasible. The online switching experiments indicate that the proposed method is feasible, and the faulty drive can realize continuous operation without downtime.

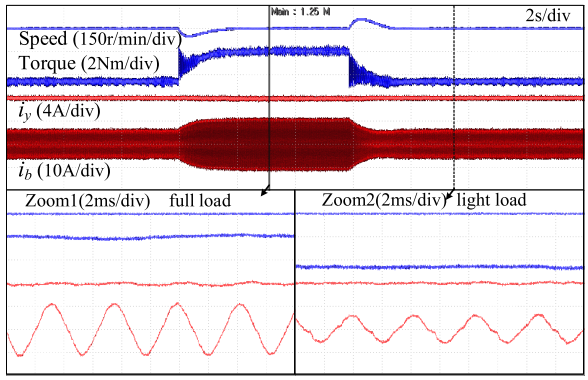

Fig. 18. Responses to external disturbance.

D. Dynamic Performance

Fig. 18 shows the dynamic responses to the external load disturbance. In this experiment, the reference speed is set to 450 r/min. The load torque is changed from 5–10–5 N·m. The waveforms of actual speed, torque, y-axis current, and phase current are recorded.

When the load torque changes, the actual speed can get back to its reference value very quickly. The harmonic currents can be restrained well under different load conditions. Moreover, the phase current exhibits good sinusoidal waveforms in different load conditions. It can be concluded that, by using the proposed method, the faulty drive has good robustness against the external load disturbance.

Fig. 19 shows the experimental result of the speedy response. In this experiment, the reference speed changes from 350–450–350 r/min. The waveforms of actual speed, phase current, and $\alpha\beta$-axis currents are depicted in Fig. 19(a). The waveforms of t harmonic current and duty cycle are shown in Fig. 19(b). According to the results, the actual speed can track the speed reference value very quickly. This means the proposed FT-MPC has good speed response. During the whole process, the $\alpha\beta$-axis currents can keep symmetry, the phase current is low distorted, and the harmonic current can be restrained. Also, in different

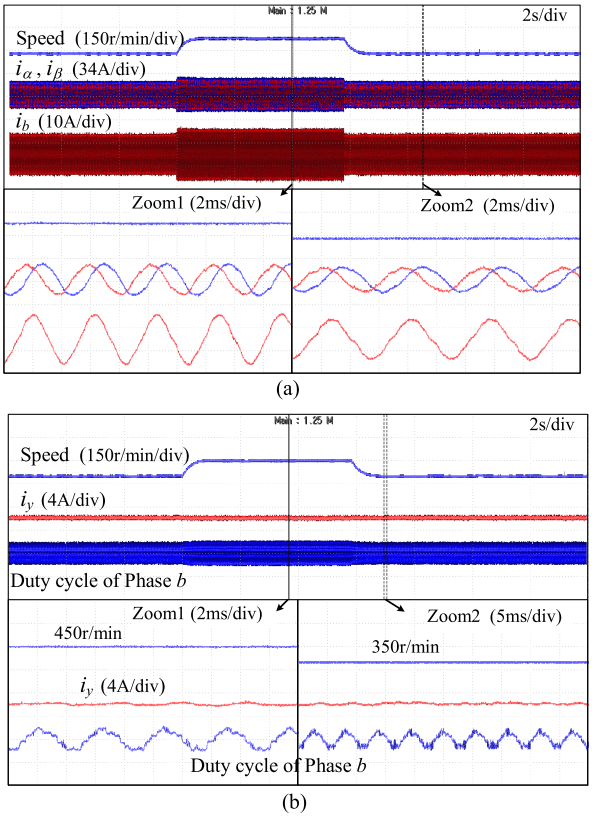

Fig. 19. Dynamic performance of speedy response. (a) Speed, phase current, and $\alpha\beta$-axis currents. (b) Speed, harmonic current, and duty cycle.

work conditions, the calculated duty cycle is consistent with the theoretical analysis.

VI. Conclusion

This article has proposed an enhanced fault-tolerant FCS-MPCC with continued modulation. By reconstructing the post-fault vector distribution, the premise of continued modulation in the fault-tolerant situation can be realized. Specifically, the reconstructed vector distribution considers the implementation of FCS-MPCC and the generation of a standard PWM waveform. The proposed fault-tolerant control can cover the full modulation area by using a multistep vector selection method. Also, the oscillation from the back EMF of the faulty phase is easy to compensate in the multistep vector selection method. A thorough experiment has been conducted to verify the proposed method. The experimental results show that the reconstructed vector distribution is effective in improving operational performance. An online switching experiment verifies the feasibility of the multistep vector selection method with the back EMF compensation. It is also verified that the proposed method has good dynamic performance and good robustness. More importantly, the faulty drive can be implemented online without downtime and maintenance.

References

[1] H. Guo, J. Xu, and Y.-H. Chen, "Robust control of fault-tolerant permanent-magnet synchronous motor for aerospace application with guaranteed fault switch process," *IEEE Trans. Ind. Electron.*, vol. 62, no. 12, pp. 7309–7321, Dec. 2015.

[2] B. Sen and J. Wang, "Stationary frame fault-tolerant current control of polyphase permanent-magnet machines under open-circuit and short-circuit faults," *IEEE Trans. Power Electron.*, vol. 31, no. 7, pp. 4684–4696, Jul. 2016.

[3] Q. Chen, W. Zhao, G. Liu, and Z. Lin, "Extension of virtual-signal-injection-based MTPA control for five-phase IPMSM into fault-tolerant operation," *IEEE Trans. Ind. Electron.*, vol. 66, no. 2, pp. 944–955, Feb. 2019.

[4] H. Lu, J. Li, R. Qu, D. Ye, and Y. Lu, "Fault-tolerant predictive control of six-phase PMSM drives based on pulsewidth modulation," *IEEE Trans. Ind. Electron.*, vol. 66, no. 7, pp. 4992–5003, Jul. 2019.

[5] A. Mohammadpour and L. Parsa, "A unified fault-tolerant current control approach for five-phase PM motors with trapezoidal back EMF under different stator winding connections," *IEEE Trans. Power Electron.*, vol. 28, no. 7, pp. 3517–3527, Jul. 2013.

[6] A. Mohammadpour, S. Sadeghi, and L. Parsa, "A generalized fault-tolerant control strategy for five-phase PM motor drives considering star, pentagon, and pentacle connections of stator windings," *IEEE Trans. Power Electron.*, vol. 61, no. 1, pp. 63–75, Jan. 2014.

[7] F. Locment, E. Semail, and X. Kestelyn, "Vectorial approach-based control of a seven-phase axial flux machine designed for fault operation," *IEEE Trans. Ind. Electron.*, vol. 55, no. 10, pp. 3682–3691, Oct. 2008.

[8] Z. Sun, J. Wang, G. W. Jewell, and D. Howe, "Enhanced optimal torque control of fault-tolerant PM machine under flux-weakening operation," *IEEE Trans. Ind. Electron.*, vol. 57, no. 1, pp. 344–353, Jan. 2010.

[9] A. Tani, M. Mengoni, L. Zarri, G. Serra, and D. Casadei, "Control of multiphase induction motors with an odd number of phases under open-circuit phase faults," *IEEE Trans. Power Electron.*, vol. 27, no. 2, pp. 565–577, Feb. 2012.

[10] H. S. Che, M. J. Duran, E. Levi, M. Jones, W.-P. Hew, and N. A. Rahim, "Postfault operation of an asymmetrical six-phase induction machine with single and two isolated neutral points," *IEEE Trans. Power Electron.*, vol. 29, no. 10, pp. 5406–5416, Oct. 2014.

[11] L. Cheng, Y. Sui, P. Zheng, P. Wang, and F. Wu, "Implementation of postfault decoupling vector control and mitigation of current ripple for five-phase fault-tolerant PM machine under single-phase open-circuit fault," *IEEE Trans. Power Electron.*, vol. 33, no. 10, pp. 8623–8636, Oct. 2018.

[12] G. Liu, Z. Lin, W. Zhao, Q. Chen, and G. Xu, "Third harmonic current injection in fault-tolerant five-phase permanent-magnet motor drive," *IEEE Trans. Power Electron.*, vol. 33, no. 8, pp. 6970–6979, Aug. 2018.

[13] M. Bermudez, I. Gonzalez-Prieto, F. Barrero, H. Guzman, X. Kestelyn, and M. J. Duran, "An experimental assessment of open-phase fault-tolerant virtual-vector-based direct torque control in five-phase induction motor drives," *IEEE Trans. Power Electron.*, vol. 33, no. 3, pp. 2774–2784, Mar. 2018.

[14] M. Bermudez, I. Gonzalez-Prieto, F. Barrero, H. Guzman, M. J. Duran, and X. Kestelyn, "Open-phase fault-tolerant direct torque control technique for five-phase induction motor drives," *IEEE Trans. Ind. Electron.*, vol. 64, no. 2, pp. 902–911, Feb. 2017.

[15] H. Zhou, C. Zhou, W. Tao, J. Wang, and G. Liu, "Virtual-stator-flux-based direct torque control of five-phase fault-tolerant permanent-magnet motor with open-circuit fault," *IEEE Trans. Power Electron.*, vol. 35, no. 5, pp. 5007–5017, May 2020.

[16] H. Guzman, M. J. Duran, F. Barrero, B. Bogado, and S. Toral, "Speed control of five-phase induction motors with integrated open-phase fault operation using model-based predictive current control techniques," *IEEE Trans. Ind. Electron.*, vol. 61, no. 9, pp. 4474–4484, Sep. 2014.

[17] H. Lu, J. Li, R. Qu, and D. Ye, "Fault-tolerant predictive current control with two-vector modulation for six-phase permanent magnet synchronous machine drives," *IET Electr. Power Appl.*, vol. 12, no. 2, pp. 169–178, Feb. 2018.

[18] T. Tao, W. Zhao, Y. Du, Y. Chen, and J. Zhu, "Simplified fault-tolerant model predictive control for a five-phase permanent-magnet motor with reduced computation burden," *IEEE Trans. Power Electron.*, vol. 35, no. 4, pp. 3850–3858, Apr. 2020.

[19] W. Huang, W. Hua, F. Chen, M. Hu, and J. Zhu, "Model predictive torque control with SVM for five-phase PMSM under open-circuit fault condition," *IEEE Trans. Power Electron.*, vol. 35, no. 5, pp. 5531–5540, May 2020.

[20] D. Zhou, P. Tu, and Y. Tang, "Multivector model predictive power control of three-phase rectifiers with reduced power ripples under nonideal grid conditions," *IEEE Trans. Ind. Electron.*, vol. 65, no. 9, pp. 6850–6859, Sep. 2018.
[21] L. Tarisciotti, P. Zanchetta, A. Watson, J. C. Clare, M. Degano, and S. Bifaretti, "Modulated model predictive control for a three-phase active rectifier," *IEEE Trans. Ind. Appl.*, vol. 51, no. 2, pp. 1610–1620, Mar./Apr. 2015.
[22] W. Zhao, T. Tao, J. Zhu, H. Tan, and Y. Du, "A novel-finite-control-set model predictive current control for five-phase PM motor with continued modulation," *IEEE Trans. Power Electron.*, vol. 35, no. 7, pp. 7261–7270, Jul. 2020.
[23] S. Vazquez, J. Rodriguez, M. Rivera, L. G. Franquelo, and M. Norambuena, "Model predictive control for power converters and drives: Advances and trends," *IEEE Trans. Ind. Electron.*, vol. 64, no. 2, pp. 935–947, Feb. 2017.
[24] M. G. Judewicz, S. A. González, N. I. Echeverría, J. R. Fischer, and D. O. Carrica, "Generalized predictive current control (GPCC) for grid-tie three-phase inverters," *IEEE Trans. Ind. Electron.*, vol. 63, no. 7, pp. 4475–4484, Jul. 2016.
[25] Z. Zhou, C. Xia, Y. Yan, Z. Wang, and T. Shi, "Torque ripple minimization of predictive torque control for PMSM with extended control set," *IEEE Trans. Ind. Electron.*, vol. 64, no. 9, pp. 6930–6939, Sep. 2017.

Tao Tao received the B.Sc. degree in electrical engineering from Nanjing Agricultural University, Nanjing, China, in 2009. He is currently working toward the Ph.D. degree in electrical engineering with Jiangsu University, Zhenjiang, China.

His research interest focuses on the control of multiphase permanent-magnet machines.

Wenxiang Zhao (Senior Member, IEEE) received the B.Sc. and M.Sc. degrees from Jiangsu University, Zhenjiang, China, in 1999 and 2003, respectively, and the Ph.D. degree from Southeast University, Nanjing, China, in 2010, all in electrical engineering.

Since 2003, he has been with Jiangsu University, where he is currently a Professor with the School of Electrical Information Engineering. From 2008 to 2009, he was a Research Assistant with the Department of Electrical and Electronic Engineering, University of Hong Kong, Hong Kong. From 2013 to 2014, he was a Visiting Professor with the Department of Electronic and Electrical Engineering, University of Sheffield, Sheffield, U.K. His current research interests include electric machine design, modeling, fault analysis, and intelligent control. He has authored and coauthored more than 200 technical papers in these areas.

Yang He received the B.Sc. degree in electronic information science and technology from Jiangsu University, Zhenjiang, China, in 2009, and the Ph.D. degree in computer science and technology from Tsinghua University, Beijing, China, in 2017.

From 2017 to 2019, he was with Tsinghua University, Beijing, China, where he was a Postdoctoral and an Assistant Research Fellow. Since 2020, he has been with Jiangsu University, where he is currently an Associate Professor. His research interests include motor control and servo control.

Yu Cheng received the B.Sc. and M.Sc. degrees in electrical engineering from Jiangsu University, Zhenjiang, China, in 2017 and 2020, respectively.

His research interest focuses on control of the linear permanent magnet vernier motor-drive system.

Suleman Saeed received the B.Sc. degree in electrical engineering from COMSATS University Islamabad, Islamabad, Pakistan, in 2018. He is currently working toward the M.Sc. degree in electrical engineering with Jiangsu University, Zhenjiang, China.

His research interests include multiphase machine drives and power electronics.

Jihong Zhu received the B.Sc. degree in electrical engineering from Jiangsu University, Zhenjiang, China, in 1990, and the Ph.D. degree in control engineering from the Nanjing University of Science and Technology, Nanjing, China, in 1995.

From 1996 to 1997, he was with the Nanjing University of Aeronautics and Astronautics, Nanjing, China, where he was a Postdoctor and an Associate Professor. Since 1998, he has been with Tsinghua University, Beijing, China, where he is currently a Professor. His teaching and research interests include motor control and flight control. He has authored or coauthored more than 150 technical papers and is the holder of more than 60 patents in these areas.